A Numerical Method for Fluid Flows with Complex Free Surfaces

Andrea Bonito[1*] and Alexandre Caboussat[2], Marco Picasso[3], and Jacques Rappaz[3]

[1] Department of Mathematics, University of Maryland, College Park, MD 20742-4015, USA andrea.bonito@a3.epfl.ch
[2] Department of Mathematics, University of Houston, 77204-3008, Houston, TX, USA caboussat@math.uh.edu
[3] Institute of Analysis and Scientific Computing, Ecole Polytechnique Fédérale de Lausanne, 1015 Lausanne, Switzerland {marco.picasso;jacques.rappaz}@epfl.ch

Summary. A numerical method for the simulation of fluid flows with complex free surfaces is presented. The liquid is assumed to be a Newtonian or a viscoelastic fluid. The compressible effects of the surrounding gas are taken into account, as well as surface tension forces. An Eulerian approach based on the volume-of-fluid formulation is chosen. A time splitting algorithm, together with a two-grids method, allows the various physical phenomena to be decoupled. A chronological approach is adopted to highlight the successive improvements of the model and the wide range of applications. Numerical results show the potentialities of the method.

1 Introduction

Complex free surface phenomena involving Newtonian and/or non-Newtonian flows are nowadays a topic of active research in many fields of physics, engineering or bioengineering. The literature contains numerous models for complex liquid-gas free surfaces problems, see, e.g., [FCD+06, SZ99]. For instance, when considering the injection of a liquid in a complex cavity initially filled with gas, an Eulerian approach is generally adopted in order to catch the topology changes of the liquid region.

Such two-phases flows are computationally expensive in three space dimensions since (at least) both the velocity and pressure must be computed at each grid point of the whole liquid-gas domain.

The purpose of this article is to review a numerical model in order to compute complex free surface flows in three space dimensions. The features

* Partially supported by the Swiss National Science Foundation Fellowship PBEL2–114311

of the model are the following. A volume-of-fluid method is used to track the liquid domain, which can exhibit complex topology changes. The velocity field is computed only in the liquid region. The incompressible liquid can be modeled either as a Newtonian or as a viscoelastic fluid. The ideal gas law is used to compute the external pressure in the surrounding gas and the resulting force is added on the liquid-gas free surface. Surface tension effects can also be taken into account on the liquid-gas free surface. The complete description of the model can be found in [MPR99, MPR03, CPR05, Cab06, BPL06].

The numerical model is based on a time-splitting approach [Glo03] and a two-grids method. This allows advection, diffusion and viscoelastic phenomena to be decoupled, as well as the treatment of the liquid and gas phases. Finite element techniques [FF92] are used to solve the diffusion phenomena using an unstructured mesh of the cavity containing the liquid. A forward characteristic method [Pir89] on a structured grid allows advection phenomena to be solved efficiently.

The article is structured as follows. In Section 2, the simplest model is presented: the liquid is an incompressible Newtonian fluid, the effects of the surrounding gas and surface tension are neglected. The effects of the surrounding gas are described in Section 3, those of the surface tension in Section 4. Finally, the case of a viscoelastic liquid is considered in Section 5. Numerical results are presented throughout the text and illustrate the capabilities and improvements of the model.

2 Modeling of an Incompressible Newtonian Fluid with a Free Surface

2.1 Governing Equations

The model presented in this section has already been published in [MPR99, MPR03]. Let Λ, with a boundary $\partial\Lambda$, be a cavity of $\mathbb{R}^3$ in which a liquid must be confined, and let $T > 0$ be the final time of simulation. For any given time $t \in (0, T)$, let Ω_t, with a boundary $\partial\Omega_t$, be the domain occupied by the liquid, let $\Gamma_t = \partial\Omega_t \setminus \partial\Lambda$ be the free surface between the liquid and the surrounding gas and let Q_T be the space-time domain containing the liquid, i.e. $Q_T = \{(x, t) : x \in \Omega_t,\ 0 < t < T\}$.

In the liquid region, the velocity field $\mathbf{v} : Q_T \to \mathbb{R}^3$ and the pressure field $p : Q_T \to \mathbb{R}$ are assumed to satisfy the time-dependent, incompressible Navier–Stokes equations, that is

$$\rho \frac{\partial \mathbf{v}}{\partial t} + \rho(\mathbf{v} \cdot \nabla)\mathbf{v} - 2\,\mathrm{div}\,(\mu \mathbf{D}(\mathbf{v})) + \nabla p = \mathbf{f} \quad \text{in } Q_T, \tag{1}$$

$$\mathrm{div}\,\mathbf{v} = 0 \quad \text{in } Q_T. \tag{2}$$

Here $\mathbf{D}(\mathbf{v}) = 0.5 \cdot (\nabla\mathbf{v} + \nabla\mathbf{v}^T)$ denotes the rate of deformation tensor, ρ the constant density and $\mathbf{f}$ the external forces.

The dynamic viscosity μ can be constant or, in order to take into account turbulence effects, a turbulent viscosity $\mu_T = \mu_T(\mathbf{v}) = \alpha_T \rho \sqrt{2\mathbf{D}(\mathbf{v}) : \mathbf{D}(\mathbf{v})}$, where α_T is a parameter to be chosen, is added. The use of a turbulent viscosity is required when large Reynolds numbers and thin boundary layers are involved. Otherwise, in order to consider Bingham flows (when considering mud flows or avalanches, for instance), a plastic viscosity $\mu_B = \alpha_0 \rho / \sqrt{2\mathbf{D}(\mathbf{v}) : \mathbf{D}(\mathbf{v})}$, where α_0 is a parameter to be chosen, can be added.

Let $\varphi : \Lambda \times (0,T) \to \mathbb{R}$ be the characteristic function of the liquid domain Q_T. The function φ equals one if the liquid is present, zero if it is not, thus $\Omega_t = \{x \in \Lambda : \varphi(x,t) = 1\}$. In order to describe the kinematics of the free surface, φ must satisfy (in a weak sense)

$$\frac{\partial \varphi}{\partial t} + \mathbf{v} \cdot \nabla \varphi = 0 \quad \text{in } \Lambda \times (0,T), \tag{3}$$

where the velocity $\mathbf{v}$ is extended continuously in the neighborhood of Q_T. At initial time, the characteristic function of the liquid domain φ is given, which defines the initial liquid region $\Omega_0 = \{x \in \Lambda : \varphi(x,0) = 1\}$. The initial velocity field $\mathbf{v}$ is prescribed in Ω_0.

The boundary conditions for the velocity field are the following. On the boundary of the liquid region being in contact with the walls (that is to say the boundary of Λ), inflow, slip or Signorini boundary conditions are enforced, see [MPR99, MPR03]. On the free surface Γ_t, the forces acting on the free surface are assumed to vanish, when both the influence of the external media and the capillary and surface tension effects are neglected on the free surface. If these influences are not neglected, we have to establish the equilibrium of forces on the free surface. In the first case, the following equilibrium relation is then satisfied on the liquid-gas interface:

$$-p\mathbf{n} + 2\mu \mathbf{D}(\mathbf{v})\mathbf{n} = 0 \quad \text{on } \Gamma_t,\ t \in (0,T), \tag{4}$$

where $\mathbf{n}$ is the unit normal of the liquid-gas free surface oriented toward the external gas.

The mathematical description of our model is complete. The model unknowns are the characteristic function φ in the whole cavity, the velocity $\mathbf{v}$ and pressure p in the liquid domain only. These unknowns satisfy the equations (1)–(3). Simplified problems extracted from this model of incompressible liquid flow with a free surface have been investigated theoretically in [CR05, Cab05], in one and two dimensions of space, and existence results and error estimates have been obtained.

2.2 Time Splitting Scheme

An implicit splitting algorithm is proposed to solve (1)–(3) by splitting the advection from the diffusion part of the Navier–Stokes equations. Let $0 = t^0 < t^1 < t^2 < \ldots < t^N = T$ be a subdivision of the time interval $[0,T]$, define

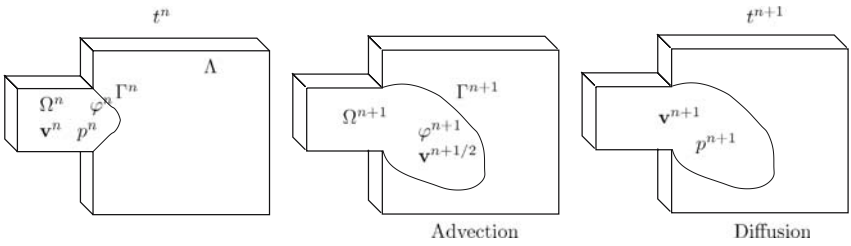

Fig. 1. The splitting algorithm (from left to right). Two advection problems are solved to determine the new approximation of the characteristic function φ^{n+1}, the new liquid domain Ω^{n+1} and the predicted velocity $\mathbf{v}^{n+1/2}$. Then, a generalized Stokes problem is solved in the new liquid domain Ω^{n+1} in order to obtain the velocity $\mathbf{v}^{n+1}$ and the pressure p^{n+1}.

$\delta t^n = t^{n+1} - t^n$ the n-th time step, $n = 0, 1, 2, \ldots, N$, δt the largest time step. Let φ^n, $\mathbf{v}^n$, p^n, Ω^n be approximations of φ, $\mathbf{v}$, p, Ω_t at time t^n, respectively. Then the approximations φ^{n+1}, $\mathbf{v}^{n+1}$, p^{n+1}, Ω^{n+1} at time t^{n+1} are computed by means of an implicit splitting algorithm, as illustrated in Figure 1.

Two advection problems are solved first, leading to a prediction of the new velocity $\mathbf{v}^{n+1/2}$ together with the new approximation of the characteristic function φ^{n+1} at time t^{n+1}, which allows to determine the new liquid domain Ω^{n+1} and the new liquid interface Γ^{n+1}. Then a generalized Stokes problem is solved on Ω^{n+1} with the boundary condition (4) on the liquid interface Γ^{n+1}, Dirichlet, slip or Signorini-type conditions on the boundary of the cavity Λ and the velocity $\mathbf{v}^{n+1}$ and pressure p^{n+1} in the liquid are obtained.

This time-splitting algorithm introduces an additional error on the velocities and pressures which is of order $\mathcal{O}(\delta t)$, see, e.g., [Mar90]. This algorithm allows the motion of the free surface to be decoupled from the diffusion step, which consists in solving a Stokes problem in a fixed domain [Glo03].
Advection Step. Solve between the times t^n and t^{n+1} the two advection problems:

$$\frac{\partial \mathbf{v}}{\partial t} + (\mathbf{v} \cdot \nabla)\mathbf{v} = 0, \quad \frac{\partial \varphi}{\partial t} + \mathbf{v} \cdot \nabla \varphi = 0 \tag{5}$$

with initial conditions $\mathbf{v}^n$ and φ^n. This step is solved exactly by the method of characteristics [Mau96, Pir89] which yields a prediction of the velocity $\mathbf{v}^{n+1/2}$ and the characteristic function of the new liquid domain φ^{n+1}:

$$\mathbf{v}^{n+1/2}(x + \delta t^n \mathbf{v}^n(x)) = \mathbf{v}^n(x) \quad \text{and} \quad \varphi^{n+1}(x + \delta t^n \mathbf{v}^n(x)) = \varphi^n(x) \tag{6}$$

for all x belonging to Ω^n. Then, the new liquid domain Ω^{n+1} is defined as the set of points such that φ^{n+1} equals one.

Diffusion Step. The diffusion step consists in solving a generalized Stokes problem on the domain Ω^{n+1} using the predicted velocity $\mathbf{v}^{n+1/2}$ and the boundary condition (4). The following backward Euler scheme is used:

$$\rho \frac{\mathbf{v}^{n+1} - \mathbf{v}^{n+1/2}}{\delta t^n} - 2\,\mathrm{div}\left(\mu \mathbf{D}(\mathbf{v}^{n+1})\right) + \nabla p^{n+1} = \mathbf{f}(t^{n+1}) \quad \text{in } \Omega^{n+1}, \tag{7}$$

$$\mathrm{div}\,\mathbf{v}^{n+1} = 0 \quad \text{in } \Omega^{n+1}, \tag{8}$$

where $\mathbf{v}^{n+1/2}$ is the prediction of the velocity obtained with (6) after the advection step. The boundary conditions on the free surface are given by (4). The weak formulation corresponding to (7), (8) and (4), therefore, consists in finding $\mathbf{v}^{n+1}$ and p^{n+1} such that $\mathbf{v}^{n+1}$ is vanishing on $\partial\Lambda$ and

$$\rho \int_{\Omega^{n+1}} \frac{\mathbf{v}^{n+1} - \mathbf{v}^{n+1/2}}{\delta t^n} \cdot \mathbf{w}\, d\mathbf{x} + 2 \int_{\Omega^{n+1}} \mu \mathbf{D}(\mathbf{v}^{n+1}) : \mathbf{D}(\mathbf{w})\, d\mathbf{x} - \int_{\Omega^{n+1}} p^{n+1}\, \mathrm{div}\,\mathbf{w}\, d\mathbf{x} - \int_{\Omega^{n+1}} \mathbf{f} \cdot \mathbf{w}\, d\mathbf{x} - \int_{\Omega^{n+1}} q\, \mathrm{div}\,\mathbf{v}^{n+1}\, d\mathbf{x} = 0, \tag{9}$$

for all test functions $(\mathbf{w}, q)$ such that $\mathbf{w}$ vanishes on the boundary of the cavity where essential boundary conditions are enforced.

2.3 A Two-Grids Method for Space Discretization

Advection and diffusion phenomena being now decoupled, the equations (5) are first solved using the method of characteristics on a structured mesh of small cells in order to reduce numerical diffusion of the interface Γ_t between the liquid and the gas, and have an accurate approximation of the liquid region, see Figure 2 (left).

The bounding box of the cavity Λ is meshed into a structured grid made out of small cubic cells of size h, each cell being labeled by indices (ijk). Let φ^n_{ijk} and $\mathbf{v}^n_{ijk}$ be the approximate values of φ and $\mathbf{v}$ at the center of cell number (ijk) at time t^n. The unknown φ^n_{ijk} is the volume fraction of liquid in the cell ijk and is the numerical approximation of the characteristic function φ at

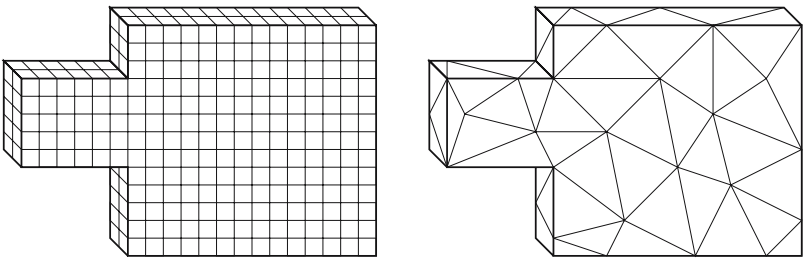

Fig. 2. Two-grids method. The advection step is solved on a structured mesh of small cubic cells composed of blocks whose union covers the physical domain Ω_h (left), while the diffusion step is solved on a finite element unstructured mesh of tetrahedra (right).

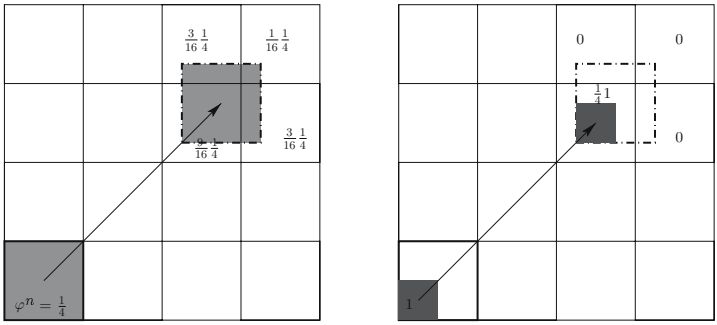

Fig. 3. Effect of the SLIC algorithm on numerical diffusion. An example of two dimensional advection and projection when the volume fraction of liquid in the cell is $\varphi^n_{ij} = \frac{1}{4}$. Left: without SLIC, the volume fraction of liquid is advected and projected on four cells, with contributions (from the top left cell to the bottom right cell) $\frac{3}{16}\frac{1}{4}$, $\frac{1}{16}\frac{1}{4}$,$\frac{9}{16}\frac{1}{4}$, $\frac{3}{16}\frac{1}{4}$. Right: with SLIC, the volume fraction of liquid is first pushed at one corner, then it is advected and projected on one cell only, with contribution $\frac{1}{4}$.

time t^n, which is piecewise constant on each cell of the structured grid. The advection step for the cell number (ijk) consists in advecting φ^n_{ijk} and $\mathbf{v}^n_{ijk}$ by $\delta t^n \mathbf{v}^n_{ijk}$ and then projecting the values on the structured grid, to obtain φ^{n+1}_{ijk} and a prediction of the velocity $\mathbf{v}^{n+\frac{1}{2}}_{ijk}$. A simple implementation of the SLIC (Simple Linear Interface Calculation) algorithm, described in [MPR03] and inspired by [NW76], allows to reduce the numerical diffusion of the domain occupied by the liquid by pushing the fluid along the faces of the cell before advecting it. The choice of how to push the fluid depends on the volume fraction of liquid of the neighboring cells. The cell advection and projection with SLIC algorithm are presented in Figure 3, in two space dimensions for the sake of simplicity. We refer to [AMS04] for a recent improvement of the SLIC algorithm.

Remark 1. A post-processing technique allows to avoid the *compression effects* and guarantees the conservation of the mass of liquid. Related to *global repair algorithms* [SW04], this technique produces final values φ^{n+1}_{ijk} which are between zero and one, even when the advection of φ^n gives values strictly larger than one. The technique consists in moving the fraction of liquid in excess in the cells that are over-filled to *receiver* cells in a global manner by sorting the cells according to φ^{n+1}. Details can be found in [MPR99, MPR03].

Once values φ^{n+1}_{ijk} and $\mathbf{v}^{n+1/2}_{ijk}$ have been computed on the cells, values of the fraction of liquid φ^{n+1}_P and of the velocity field $\mathbf{v}^{n+\frac{1}{2}}_P$ are computed at the nodes P of the finite element mesh with approximated projection methods. We take advantage of the difference of refinement between a coarse finite element

mesh and a finer structured grid of cells. Let $\mathcal{T}_h$ be the triangulation of the cavity Λ. For any vertex P of $\mathcal{T}_h$, let ψ_P be the corresponding finite element basis function (i.e. the continuous, piecewise linear function having value one at P, zero at the other vertices). Then, φ_P^{n+1}, the volume fraction of liquid at vertex P and time t^{n+1} is computed by:

$$\varphi_P^{n+1} = \left(\sum_{\substack{K \in \mathcal{T}_h \\ P \in K}} \sum_{\substack{ijk \\ C_{ijk} \in K}} \psi_P(C_{ijk}) \varphi_{ijk}^{n+1} \right) / \left(\sum_{\substack{K \in \mathcal{T}_h \\ P \in K}} \sum_{\substack{ijk \\ C_{ijk} \in K}} \psi_P(C_{ijk}) \right), \quad (10)$$

where C_{ijk} is the center of the cell (ijk). The same kind of formula is used to obtain the predicted velocity $\mathbf{v}^{n+\frac{1}{2}}$ at the vertices of the finite element mesh. When these values are available at the vertices of the finite element mesh, the approximation of the liquid region Ω_h^{n+1} used for solving (9) is defined as the union of all elements of the mesh $K \in \mathcal{T}_h$ with (at least) one of its vertices P such that $\varphi_P^{n+1} > 0.5$, the approximation of the free surface being denoted by Γ_h^{n+1}.

Numerical experiments reported in [MPR99, MPR03] have shown that choosing the size of the cells of the structured mesh approximately 5 to 10 times smaller than the size of the finite elements is a good choice to reduce numerical diffusion of the interface Γ_t. Furthermore, since the characteristics method is used, the time step is not restricted by the CFL number (which is the ratio between the time step times the maximal velocity divided by the mesh size). Numerical results in [MPR99, MPR03] have shown that a good choice generally consists in choosing CFL numbers ranging from 1 to 5.

Remark 2. In number of industrial mold filling applications, the shape of the cavity containing the liquid (the mold) is complex. Therefore, a special, hierarchical, data structure has been implemented in order to reduce the memory requirements, see [MPR03, RDG+00]. The cavity is meshed into tetrahedra for the resolution of the diffusion problem. For the advection part, a hierarchical structure of blocks, which cover the cavity and are glued together, is defined. A computation is performed inside a block if and only if it contains cells with liquid. Otherwise the whole block is deactivated.

The diffusion step consists in solving the Stokes problem (9) with finite element techniques. Let $\mathbf{v}_h^{n+1}$ (resp. p_h^{n+1}) be the piecewise linear approximation of $\mathbf{v}^{n+1}$ (resp. p^{n+1}). The Stokes problem is solved with stabilized $\mathbb{P}_1 - \mathbb{P}_1$ finite elements (Galerkin Least Squares, see [FF92]) and consists in finding the velocity $\mathbf{v}_h^{n+1}$ and pressure p_h^{n+1} such that:

$$\rho \int_{\Omega_h^{n+1}} \frac{\mathbf{v}_h^{n+1} - \mathbf{v}_h^{n+1/2}}{\delta t^n} \mathbf{w}\, d\mathbf{x} + 2 \int_{\Omega_h^{n+1}} \mu \mathbf{D}(\mathbf{v}_h^{n+1}) : \mathbf{D}(\mathbf{w})\, d\mathbf{x}$$
$$- \int_{\Omega_h^{n+1}} \mathbf{f}\mathbf{w}\, d\mathbf{x} - \int_{\Omega_h^{n+1}} p_h^{n+1} \operatorname{div} \mathbf{w}\, d\mathbf{x} - \int_{\Omega_h^{n+1}} \operatorname{div} \mathbf{v}_h^{n+1} q\, d\mathbf{x}$$
$$- \sum_{K \subset \Omega_h^{n+1}} \alpha_K \int_K \left(\frac{\mathbf{v}_h^{n+1} - \mathbf{v}_h^{n+1/2}}{\delta t^n} + \nabla p_h^{n+1} - \mathbf{f} \right) \cdot \nabla q\, d\mathbf{x} = 0, \quad (11)$$

for all $\mathbf{w}$ and q the velocity and pressure test functions, compatible with the boundary conditions on the boundary of the cavity Λ. The value of the parameter α_K is discussed in [MPR99, MPR03].

The projection of the continuous piecewise linear approximation $\mathbf{v}_h^{n+1}$ back on the cell (ijk) is obtained by interpolation of the piecewise finite element approximation at the center C_{ijk} of the cell. It allows to obtain a value of the velocity $\mathbf{v}_{ijk}^{n+1}$ on each cell ijk of the structured grid for the next time step.

2.4 Numerical Results

The classical "vortex-in-a-box" test case widely treated in the literature is considered here [RK98]. The initial liquid domain is a circle of radius 0.015 with its center located in $(0.05, 0.075)$. It is stretched by a given velocity, given by the stream function $\psi(x, y) = 0.01\pi \sin^2(\pi x/0.1) \sin^2(\pi y/0.1) \cos(\pi t/2)$. The velocity being periodic in time, the initial liquid domain is reached after a time $T = 2$. Figure 4 illustrates the liquid-gas interface for three structured meshes [CPR05]. The interface with maximum deformation and the interface after one period of time are represented. Numerical results show the efficiency and convergence of the scheme.

An S-shaped channel lying between two horizontal plates is filled. The channel is contained in a $0.17\,\mathrm{m} \times 0.24\,\mathrm{m}$ rectangle. The distance between the two horizontal plates is $0.008\,\mathrm{m}$. Water is injected at one end with

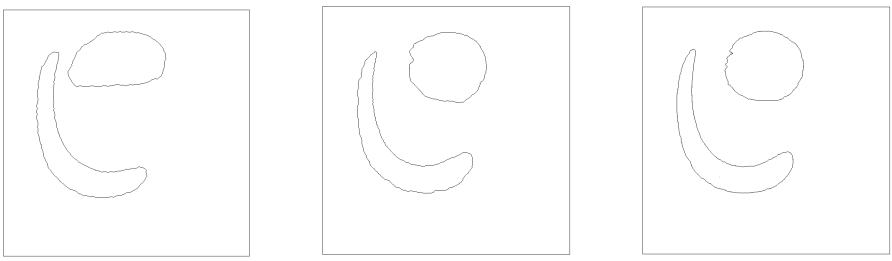

Fig. 4. Single vortex test case, representation of the computed interface at times $t = 1$ (maximal deformation) and $t = 2$ (return to initial shape). Left: coarser mesh, middle: middle mesh, right: finer mesh.

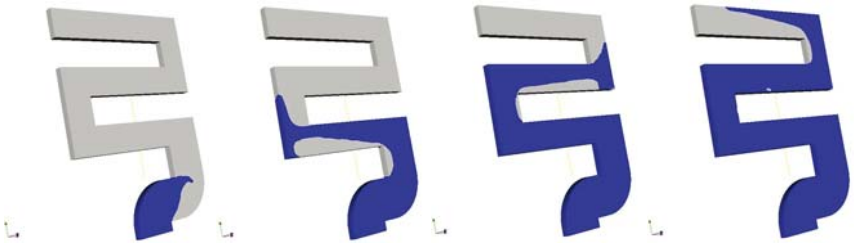

Fig. 5. S-shaped channel: 3D results when the cavity is initially filled with vacuum. Time equals 8.0 ms, 26.0 ms, 44.0 ms and 53.9 ms.

constant velocity 8.7 m/s. Density and viscosity are taken to be respectively $\rho = 1000\,\mathrm{kg/m^3}$ and $\mu = 0.01\,\mathrm{kg/(ms)}$.

Slip boundary conditions are enforced to avoid boundary layers and a turbulent viscosity is added, the coefficient α_T being equal to $4h^2$, as proposed in [CPR05]. Since the ratio between Capillary number and Reynolds number is very small, surface tension effects are neglected.

The final time is $T = 0.0054$ s and the time step is $\tau = 0.0001$ s. The mesh is made out of 96030 elements. In Figure 5, 3D computations are presented when a valve is placed at the end of the cavity, thus allowing the gas to exit. The CPU time for the simulations in three space dimensions is approximately 319 minutes for 540 time steps. Most of the CPU time is spent to solve the Stokes problem. A comparison with experimental results shows that the bubbles of gas trapped by the liquid vanish too rapidly. In order to obtain more realistic results, the effect of the gas compressibility onto the liquid must be considered. This is the scope of the next section.

3 Extension to the Modeling of an Incompressible Liquid Surrounded by a Compressible Gas

3.1 Extension of the Model

In Section 2, the zero force condition (4) was applied on the liquid-gas interface. Going back to the simulation of Figure 5, this corresponds to filling with liquid a cavity under vacuum. When considering industrial mold filling processes, the mold is not initially under vacuum, but contains some compressible air that interacts with the liquid. Therefore, the model has to be extended. The velocity in the gas is disregarded here, since it is CPU time consuming to solve the Euler compressible equations in the gas domain. The model presented in Section 2 is extended by adding the normal forces due to the gas pressure on the free surface Γ_t, still neglecting tangential and capillary forces. The relationship (4) is replaced by

$$-p\mathbf{n} + 2\mu\mathbf{D}(\mathbf{v})\mathbf{n} = -P\mathbf{n} \quad \text{on } \Gamma_t,\ t \in (0,T), \tag{12}$$

where P is the pressure in the gas. For instance, consider the experiment of Figure 5 where the cavity is being filled with liquid. The gas present in the cavity at initial time can either escape if a *valve* is placed at the end of the cavity (in which case the gas does exert very little resistance on the liquid) or be trapped in the cavity. When a bubble of gas is trapped by the liquid, the gas pressure prevents the bubble to vanish rapidly, as it is the case for vacuum.

The pressure in the gas is assumed to be constant in space in each bubble of gas, that is to say in each connected component of the gas domain. Let $k(t)$ be the number of bubbles of gas at time t and let $B_i(t)$ denote the domain occupied by the bubble number i (the i-th connected component). Let $P_i(t)$ denote the pressure in $B_i(t)$. At initial time, $P_i(0)$ is constant in each bubble i. The gas is assumed to be an ideal gas. If $V_i(t)$ is defined as the volume of $B_i(t)$, the pressure in each bubble at time t is thus computed by using the law of ideal gases at constant temperature:

$$P_i(t)V_i(t) = \text{constant} \quad i = 1, \ldots, k(t). \tag{13}$$

The above relationship is an expression of the conservation of the number of molecules of trapped gas (gas that cannot escape through a valve) between time t and $t + \delta t$. However, this simplified model requires the tracking of the position of the bubbles of gas between two time steps.

When δt is small enough, three situations appear between two time steps: first, a single bubble remains a single bubble; or a bubble splits into two bubbles, or two bubbles merge into one. Combinations of these three situations may appear.

For instance, in the case of a single bubble, if the pressure $P(t)$ in the bubble at time t and the volumes $V(t)$ and $V(t + \delta t)$ are known, the gas pressure at time $t+\delta t$ is easily computed from the relation $P(t+\delta t)V(t+\delta t) = P(t)V(t)$. The other cases are described at the discrete level in the following. Details can be found in [CPR05].

The additional unknowns in our model are the bubbles of gas $B_i(t)$ and the constant pressure $P = P_i(t)$ in the bubble of gas number i. The equations (1)–(3) are to be solved together with (12), (13).

3.2 Modification of the Numerical Method

The tracking of the bubbles of gas and the computation of their internal pressure introduce an additional step in our time splitting scheme. This procedure is inserted between the advection step (6) and the diffusion step (7), (8), in order to compute an approximation of the pressure to plug into (12).

Let us denote by k^n, P_i^n, B_i^n, $i = 1, 2, \ldots, k^n$, the approximations of k, P_i, B_i, $i = 1, 2, \ldots, k$, respectively at time t^n. Let $\xi(t)$ be a *bubble numbering*

function, defined as negative in the liquid region Ω_t and equal to i in bubble $B_i(t)$. The approximations k^{n+1}, P_i^{n+1}, B_i^{n+1}, $i = 1, 2, \ldots, k^{n+1}$ and ξ^{n+1} are computed as follows.

Numbering of the Bubbles of gas

Given the new liquid domain Ω^{n+1}, the key point is to find the number of bubbles k^{n+1} (that is to say the number of connected components) and the bubbles B_i^{n+1}, $i = 1, \ldots, k^{n+1}$. Given a point P in the gas domain $\Lambda \setminus \Omega^{n+1}$, we search for a function u such that $-\Delta u = \delta_P$ in $\Lambda \setminus \Omega^{n+1}$, with $u = 0$ on Ω^{n+1} and u continuous. Since the solution u to this problem is strictly positive in the connected component containing point P and vanishes outside, the first bubble is found. The procedure is repeated iteratively until all the bubbles are recognized. The algorithm is written as follows:

Set $k^{n+1} = 0$, $\xi^{n+1} = 0$ in $\Lambda \setminus \Omega^{n+1}$ and $\xi^{n+1} = -1$ in Ω^{n+1}, and $\Theta^{n+1} = \{x \in \Lambda : \xi^{n+1}(x) = 0\}$.
While $\Theta^{n+1} \neq \emptyset$, do:

1. Choose a point P in Θ^{n+1};
2. Solve the following problem: Find $u : \Lambda \to \mathbb{R}$ which satisfies:

$$\begin{cases} -\Delta u = \delta_P, & \text{in } \Theta^{n+1}, \\ u = 0, & \text{in } \Lambda \setminus \Theta^{n+1}, \\ [u] = 0, & \text{on } \partial\Theta^{n+1}, \end{cases} \tag{14}$$

   where δ_P is Dirac delta function at point P, $[u]$ is the jump of u through $\partial\Theta^{n+1}$;
3. Increase the number of bubbles k^{n+1} at time t^{n+1}: $k^{n+1} = k^{n+1} + 1$;
4. Define the bubble of gas number k^{n+1}: $B_{k^{n+1}}^{n+1} = \{x \in \Theta^{n+1} : u(x) \neq 0\}$;
5. Update the bubble numbering function $\xi^{n+1}(x) = k^{n+1}$, for all $x \in B_{k^{n+1}}^{n+1}$;
6. Update Θ^{n+1} for the next iteration: $\Theta^{n+1} = \{x \in \Lambda : \xi^{n+1}(x) = 0\}$.

The cost of this original numbering algorithm is bounded by the cost of solving k^{n+1} times a Poisson problem in the gas domain. The corresponding CPU time used to solve the Poisson problems is usually less than 10 percent of the total CPU time. This numbering algorithm is implemented on the finite element mesh. The Poisson problems (14) are solved on $\mathcal{T}_h$, using standard continuous, piecewise linear finite elements.

Computation of the Pressure in the Gas

Once the connected components of gas are numbered, an approximation P_i^{n+1} of the constant pressure in bubble i at time t^{n+1} has to be computed with (13). In the case of a single bubble in the liquid, (13) yields $P_1^{n+1}V_1^{n+1} = P_1^n V_1^n$. In the case when two bubbles merge, this relation becomes $P_1^{n+1}V_1^{n+1} = P_1^n V_1^n + P_2^n V_2^n$. When a bubble B_1^n splits onto two,

each of its parts at time t^n contributes to bubbles B_1^{n+1} and B_2^{n+1}. The volume fraction of bubble B_1^n which contributes to bubble B_j^{n+1} is noted $V_{1,j}^{n+1/2}$, $j = 1, 2$. The pressure in the bubble B_j^{n+1} is computed by taking into account the compression/decompression of the two fractions of bubbles $P_j^{n+1} = P_1^n V_{1,j}^{n+1/2} / V_j^{n+1}$, $j = 1, 2$.

Details of the implementation require to take into account several situations, when two bubbles at time t^n and t^{n+1} do or do not intersect between two time steps, and are detailed in [CPR05]. The value of the pressure can be inserted as a boundary term in (9) for the resolution of the generalized Stokes problem (7), (8).

Remark 3. By using the divergence theorem in the variational formulation (9) and the fact that P^{n+1} is piecewise constant, the integral on the free surface Γ_h^{n+1} is transformed into an integral on Ω_h^{n+1} and, therefore, an approximation of the normal vector $\mathbf{n}$ is not explicitly needed.

3.3 Numerical Results

Numerical results are presented here for mold filling simulations in order to show the influence of the gas pressure and to compare with results in Section 2.4.

The same S-shaped channel is initially filled with gas at atmospheric pressure $P = 101300\,\text{Pa}$. A valve is located at the upper extremity of the channel allowing gas to escape. Numerical results (cf. Figure 6) show the persistence of the bubbles. The CPU time for the simulations is approximately 344 min with the bubbles computations (to compare with 319 min in Section 2).

Fig. 6. S-shaped channel: 3D results when the cavity is initially filled with compressible gas at atmospheric pressure. Time equals 8.0 ms, 26.0 ms, 44.0 ms and 53.9 ms.

4 Extension to the Modeling of Incompressible Liquid-Compressible Gas Two-Phases Flows with Surface Tension Effects

4.1 Extension of the Model

Surface tension effects are usually neglected for high Reynolds numbers. However, for creeping flows (with low Reynolds number and high Capillary number), the surface tension effects become relevant. The model presented in Section 3 is extended, so that tangential and capillary forces are still neglected on the free surface, but the normal forces due to the surface tension effects are added. Details can be found in [Cab06]. The relationship (12) is replaced by

$$-p\mathbf{n} + 2\mu\mathbf{D}(\mathbf{v})\mathbf{n} = -P\mathbf{n} + \sigma\kappa\mathbf{n} \quad \text{on } \Gamma_t,\ t \in (0,T), \tag{15}$$

where $\kappa = \kappa(x,t)$ is the mean curvature of the interface Γ_t at point $x \in \Gamma_t$ and σ is a constant surface tension coefficient which depends on both media on each side of the interface (namely the liquid and the gas). The *continuum surface force* (CSF) model, see, e.g., [BKZ92, RK98, WKP99], is considered for the modeling of surface tension effects.

4.2 Modification of the Numerical Method

The relationship (15) on the interface requires the computation of the curvature κ and the normal vector $\mathbf{n}$. An additional step is added in the time splitting scheme to compute these two unknowns before the diffusion part. The approximations κ^{n+1} and $\mathbf{n}^{n+1}$ of κ and $\mathbf{n}$ respectively are computed at time t^{n+1} on the interface Γ^{n+1} as follows.

Since the characteristic function φ^{n+1} is not smooth, it is first mollified, see, e.g., [WKP99], in order to obtain a smoothed approximation $\tilde{\varphi}^{n+1}$, such that the liquid-gas interface Γ^{n+1} is given by the level line $\{x \in \Lambda : \tilde{\varphi}^{n+1}(x) = 1/2\}$, with $\tilde{\varphi}^{n+1} < 1/2$ in the gas domain and $\tilde{\varphi}^{n+1} > 1/2$ in the liquid domain. The smoothed characteristic function $\tilde{\varphi}^{n+1}$ is obtained by convolution of φ^{n+1} with the fourth-order kernel function K_ε described in [WKP99]:

$$\tilde{\varphi}^{n+1}(x) = \int_\Lambda \varphi^{n+1}(y) K_\varepsilon(x-y)\, dy \quad \forall x \in \Lambda. \tag{16}$$

The smoothing of φ^{n+1} is performed only in a layer around the free surface. The parameter ε is the smoothing parameter that describes the size of the support of K_ε, i.e. the size of the smoothing layer around the interface. At each time step, the normal vector $\mathbf{n}^{n+1}$ and the curvature κ^{n+1} on the liquid-gas interface are given respectively by $\mathbf{n}^{n+1} = -\nabla\tilde{\varphi}^{n+1}/\|\nabla\tilde{\varphi}^{n+1}\|$ and $\kappa^{n+1} = -\operatorname{div}(\nabla\tilde{\varphi}^{n+1}/\|\nabla\tilde{\varphi}^{n+1}\|)$, see, e.g., [OF01, Set96].

Instead of using the structured grid of cells to compute the curvature, see, e.g., [AMS04, SZ99], the computation of κ^{n+1} is performed on the finite element mesh, in order to use the variational framework of finite elements.

The normal vector $\mathbf{n}_h^{n+1}$ is given by the normalized gradient of $\tilde{\varphi}_h^{n+1}$ at each grid point P_j, $j = 1, \ldots, M$ where M denotes the number of nodes in the finite element discretization. Details can be found in [Cab06]. The curvature κ^{n+1} is approximated by its L^2-projection on the piecewise linear finite elements space with *mass lumping* and is denoted by κ_h^{n+1}. The basis functions of the piecewise linear finite element space associated to each node P_j in the cavity being denoted by ψ_{P_j}, κ_h^{n+1} is given by the relation

$$\int_\Lambda \kappa_h^{n+1} \psi_{P_j} \, d\mathbf{x} = \int_\Lambda - \operatorname{div} \frac{\nabla \tilde{\varphi}_h^{n+1}}{\|\nabla \tilde{\varphi}_h^{n+1}\|} \psi_{P_j} \, d\mathbf{x}, \quad \text{for all } j = 1, \ldots, M.$$

The left-hand side of this relation is computed with *mass lumping*, while the right-hand side is integrated by parts. Explicit values of the curvature of the level lines of $\tilde{\varphi}_h^{n+1}$ are obtained at the vertices of the finite element mesh being in a layer around the free surface. The restriction of κ_h^{n+1} to the nodes lying on Γ_h^{n+1} is used to compute (15).

4.3 Numerical Results

We consider a bubble of gas at the bottom of a cylinder filled with liquid, under gravity forces. The bubble rises and reaches an upper free surface between water and air, see Figure 7. The physical constants are $\mu = 0.01\,\mathrm{kg/(ms)}$, $\rho = 1000\,\mathrm{kg/m^3}$ and $\sigma = 0.0738\,\mathrm{N/m}$. The mesh made out of 115200 tetrahedra. The size of the cells of the structured mesh used for advection step is approximately 5 to 10 times smaller than the size of the finite elements and

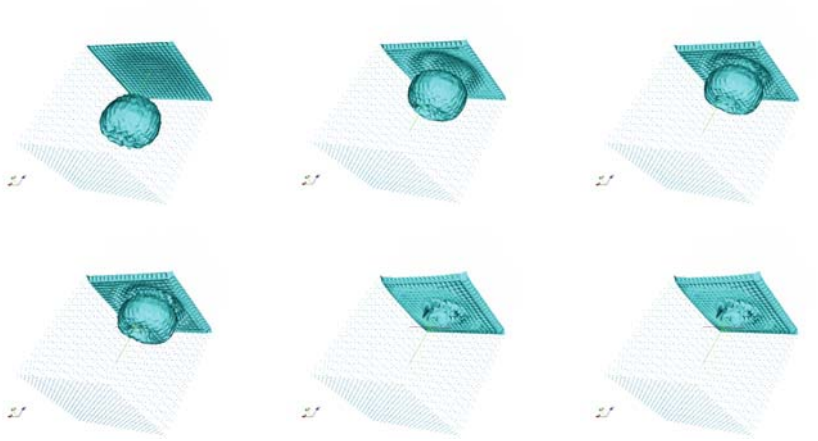

Fig. 7. Three-dimensional rising bubble under a free surface: Representation of the gas domain at times $t = 100.0, 200.0, 230.0, 240.0., 300.0$ and 320.0 ms (left to right, top to bottom).

the time step is chosen such that the CFL number is approximately one. The smoothing parameter is $\varepsilon = 0.005$. The CPU time for this computation is approximately 20 hours to achieve 1000 time steps.

5 Extension to the Modeling of Viscoelastic Flows with a Free Surface

5.1 Extension of the Model

The total stress tensor for incompressible viscoelastic fluids is, by definition, the sum of a Newtonian part $2\mu\mathbf{D}(\mathbf{v}) - p\mathbf{I}$ and a non-Newtonian part denoted by $\boldsymbol{\sigma} : Q_T \to \mathbb{R}^{3\times 3}$. Owning this decomposition, the system (1)–(2) becomes

$$\rho\frac{\partial \mathbf{v}}{\partial t} + \rho(\mathbf{v}\cdot\nabla)\mathbf{v} - 2\,\mathrm{div}\,(\mu\mathbf{D}(\mathbf{v}) + \boldsymbol{\sigma}) + \nabla p = \mathbf{f} \quad \text{in } Q_T, \tag{17}$$

$$\mathrm{div}\,\mathbf{v} = 0 \quad \text{in } Q_T. \tag{18}$$

The simplest constitutive (or closure) equation for the extra-stress $\boldsymbol{\sigma}$, namely the Oldroyd-B model [Old50], is chosen to supplement the above system

$$\boldsymbol{\sigma} + \lambda\left(\frac{\partial \boldsymbol{\sigma}}{\partial t} + (\mathbf{v}\cdot\nabla)\boldsymbol{\sigma} - (\nabla\mathbf{v})\boldsymbol{\sigma} - \boldsymbol{\sigma}(\nabla\mathbf{v})^T\right) = 2\eta\mathbf{D}(\mathbf{v}) \quad \text{in } Q_T. \tag{19}$$

Here $\lambda > 0$ is the relaxation time (the time for the stress to return to zero under constant-strain condition) and $\eta > 0$ is the polymer viscosity. The extra-stress $\boldsymbol{\sigma}$ has to be imposed only at the inflow. For more details, we refer to [BPL06].

Remark 4. The numerical procedures described in this section can be extended to more general deterministic models such as Phan-Thien Tanner [PTT77], Giesekus [Gie82] and stochastic models such as, e.g., FENE [War72], FENE-P [BDJ80]. Two-dimensional computations of free surface flows with FENE dumbbells have been performed in [GLP03].

5.2 Modification of the Numerical Procedure

The convective term in (19) is treated in the same fashion as (5). Continuous, piecewise linear finite elements are considered to approximate the extra-stress tensor $\boldsymbol{\sigma}$ and an EVSS (*Elastic Viscous Split Stress*) procedure [FGP97, BPS01, PR01] is used in order to obtain a stable algorithm even if the solvent viscosity μ vanishes.

Advection Step. Together with (5), solve between the times t^n and t^{n+1}

$$\frac{\partial \boldsymbol{\sigma}}{\partial t} + (\mathbf{u}\cdot\nabla)\boldsymbol{\sigma} = 0 \tag{20}$$

with initial conditions given by the value of the tensor $\boldsymbol{\sigma}$ at time t^n. This step is also solved using the characteristics method on the structured grid, see Figure 2, using the relation $\boldsymbol{\sigma}^{n+1/2}(x+\delta t^n \mathbf{v}^n(x)) = \boldsymbol{\sigma}^n(x)$. As for the velocity and volume fraction of liquid, the extra-stress tensor $\boldsymbol{\sigma}^{n+1/2}$ is computed on the structured grid of cells (ijk) leading to values $\boldsymbol{\sigma}_{ijk}^{n+1/2}$. Then, values are interpolated at the nodes of the finite element mesh using the same kind of formula as in (10), which yields the continuous, piecewise linear extra-stress $\boldsymbol{\sigma}_h^{n+1/2}$.

Diffusion Step. The diffusion step consists in solving the so-called three-fields Stokes problem on the finite element mesh. Following the EVSS method, we define a new extra-tensor $\mathbf{B}_h^{n+1/2} : \Omega_h^{n+1} \to \mathbb{R}^{3\times 3}$ as the L^2-projection into the finite element space of the predicted deformation tensor $\mathbf{D}(\mathbf{v}_h^{n+1/2})$, i.e.

$$\int_{\Omega_h^{n+1}} \mathbf{B}_h^{n+1/2} : \mathbf{E}_h \, d\mathbf{x} = \int_{\Omega_h^{n+1}} \mathbf{D}(\mathbf{v}_h^{n+1/2}) : \mathbf{E}_h \, d\mathbf{x},$$

for all test functions $\mathbf{E}_h$. Then (9) is modified to take explicitly into account the term coming from the extra-stress tensor. The extra term

$$2\int_{\Omega_h^{n+1}} \eta \mathbf{D}(\mathbf{v}_h^{n+1}) : \mathbf{D}(\mathbf{w}_h) \, d\mathbf{x} - 2\int_{\Omega_h^{n+1}} \eta \mathbf{B}_h^{n+1/2} : \mathbf{D}(\mathbf{w}_h) \, d\mathbf{x},$$

which vanishes at continuous level, is also added. Thus, the weak formulation (9) becomes, find the piecewise linear finite element approximations $\mathbf{v}_h^{n+1}$ and p_h^{n+1} such that $\mathbf{v}_h^{n+1}$ satisfies the essential boundary conditions on the boundary of the cavity Λ and such that

$$\begin{aligned} \rho \int_{\Omega_h^{n+1}} \frac{\mathbf{v}_h^{n+1} - \mathbf{v}_h^{n+1/2}}{\delta t^n} \cdot \mathbf{w}_h \, d\mathbf{x} + 2\int_{\Omega_h^{n+1}} (\mu+\eta) \mathbf{D}(\mathbf{v}_h^{n+1}) : \mathbf{D}(\mathbf{w}_h) \, d\mathbf{x} \\ - \int_{\Omega_h^{n+1}} p_h^{n+1} \operatorname{div} \mathbf{w}_h \, d\mathbf{x} + \int_{\Omega_h^{n+1}} \boldsymbol{\sigma}_h^{n+1/2} : \mathbf{D}(\mathbf{w}_h) \, d\mathbf{x} \\ -2\int_{\Omega_h^{n+1}} \eta \mathbf{B}_h^{n+1/2} : \mathbf{D}(\mathbf{w}_h) \, d\mathbf{x} - \int_{\Omega_h^{n+1}} \mathbf{f} \cdot \mathbf{w}_h \, d\mathbf{x} - \int_{\Omega_h^{n+1}} q_h \operatorname{div} \mathbf{v}_h^{n+1} \, d\mathbf{x} = 0, \end{aligned} \tag{21}$$

for all test functions $\mathbf{w}_h$, q_h. Once the velocity $\mathbf{v}_h^{n+1}$ is computed, the extra-stress is recovered using (19). More precisely the continuous, piecewise linear extra-stress $\boldsymbol{\sigma}_h^{n+1}$ satisfies the prescribed boundary conditions at inflow and

$$\int_{\Omega_h^{n+1}} \boldsymbol{\sigma}_h^{n+1} : \boldsymbol{\tau}_h \, d\mathbf{x} + \lambda \int_{\Omega_h^{n+1}} \frac{\boldsymbol{\sigma}_h^{n+1} - \boldsymbol{\sigma}_h^{n+1/2}}{\delta t^n} : \boldsymbol{\tau}_h \, d\mathbf{x}$$
$$= 2\eta \int_{\Omega_h^{n+1}} \mathbf{D}(\mathbf{v}_h^{n+1}) : \boldsymbol{\tau}_h \, d\mathbf{x}$$
$$+ \lambda \int_{\Omega_h^{n+1}} \left((\nabla \mathbf{v}_h^{n+1}) \boldsymbol{\sigma}_h^{n+1/2} + \boldsymbol{\sigma}_h^{n+1/2} (\nabla \mathbf{v}_h^{n+1})^T \right) : \boldsymbol{\tau}_h \, d\mathbf{x}, \quad (22)$$

for all test functions $\boldsymbol{\tau}_h$. Finally, the fields $\mathbf{u}_h^{n+1}$ and $\boldsymbol{\sigma}_h^{n+1}$ are interpolated at the center of the cells C_{ijk}.

Theoretical investigations for a simplified problem without advection and free surface have been performed in [BCP07]. Using an implicit function theorem, existence of a solution and convergence of the finite element scheme have been obtained. We refer to [BCP06b, BCP06a] for an extension to the stochastic Hookean dumbbells model.

5.3 Numerical Results

Two different simulations are provided here, the *buckling* of a jet and the stretching of a filament. In the first simulation, different behaviors between Newtonian and viscoelastic fluids are observed and the elastic effect of the relaxation time λ is pointed out. In the second simulation, *fingering instabilities* can be observed, which corresponds to experiments. More details and test cases can be found in [BPL06].

Jet buckling

The transient flow of a jet of diameter $d = 0.005$ m, injected into a parallelepiped cavity of width 0.05 m, depth 0.05 m and height 0.1 m, is reproduced. Liquid enters from the top of the cavity with vertical velocity $U = 0.5$ m/s. The fluids parameters are given in Table 1, the effects of surface tension being not considered.

The finite element mesh has 503171 vertexes and 2918760 tetrahedra. The cells size is 0.0002 m and the time step is 0.001 s thus the CFL number of the cells is 2.5. A comparison of the shape of the jet with Newtonian flow is shown in Figure 8. This computation takes 64 hours on a AMD Opteron CPU with 8Gb memory. The elastic effects in the liquid are clearly observed: when the viscoelastic jet starts to buckle, the Newtonian jet has already produced many

Table 1. Jet buckling. Liquid parameters.

	ρ [kg/m^3]	μ [Pa·s]	η [Pa·s]	λ [s]	De $= \lambda U/d$
Newtonian	1030	10.3	0	0	0
Viscoelastic	1030	1.03	9.27	1	100

Fig. 8. Jet buckling in a cavity. Shape of the jet at time $t = 0.125$ s (col. 1), $t = 0.45$ s (col. 2), $t = 0.6$ s (col. 3), $t = 0.9$ s (col. 4), $t = 1.15$ s (col. 5), $t = 1.6$ s (col. 6), Newtonian fluid (row 1), viscoelastic fluid (row 2).

folds. For a discussion on the condition for a jet to buckle and comparison with results obtained in [TMC+02], we refer to [BPL06].

Fingering instabilities

The numerical model is capable to reproduce fingering instabilities, as reported in [RH99, BRLH02, MS02, DLCB03] for non-Newtonian flows. The flow of an Oldroyd-B fluid contained between two parallel coaxial circular disks with radius $R_0 = 0.003$ m is considered. At the initial time, the distance between the two end-plates is $L_0 = 0.00015$ m and the liquid is at rest. Then, the top end-plate is moved vertically with velocity $L_0\dot{\varepsilon}_0 e^{\dot{\varepsilon}_0 t}$ where $\dot{\varepsilon}_0 = 4.68\,\mathrm{s}^{-1}$. The liquid parameters are $\rho = 1030\,\mathrm{kg/m}^3$, $\mu = 9.15\,\mathrm{Pa{\cdot}s}$, $\eta = 25.8\,\mathrm{Pa{\cdot}s}$, $\lambda = 0.421\,\mathrm{s}$. Following [MS02, Section 4.4], since the aspect ratio R_0/L_0 is equal to 20, the Weissenberg number $\mathrm{We} = \mathrm{De}R_0^2/L_0^2$ is large.

The finite element mesh has 50 vertexes along the radius and 25 vertexes along the height, thus the mesh size is 0.00006 m. The cells size is 0.00001 m and the initial time step is $\delta t = 0.01\,\mathrm{s}$ thus the CFL number of the cells is initially close to one. The shape of the filament is reported in Figure 9 and 2D cuts in the middle of the height are reported in Figure 10. Fingering instabilities can be observed from the very beginning of the stretching, leading to branched structures, as described in [MS02, BRLH02, DLCB03]. These instabilities are essentially elastic, without surface tension effects [RH99]. Clearly, such complex shapes cannot be obtained using Lagrangian models, the mesh distortion being too large.

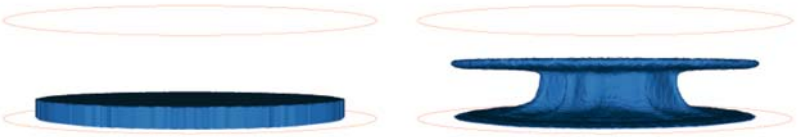

Fig. 9. Fingering instabilities. Shape of the liquid region at times $t = 0$ s (left) and $t = 0.745$ s (right).

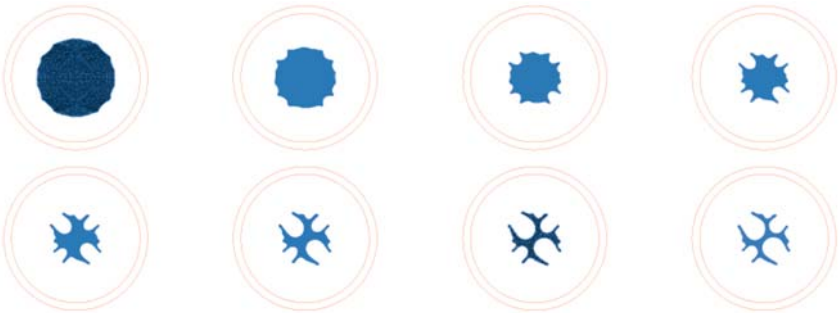

Fig. 10. Fingering instabilities. Horizontal cuts through the middle of the liquid region at times $t = 0.119$ s, $t = 0.245$ s, $t = 0.364$ s, $t = 0.49$ s (first row) and times $t = 0.609$ s, $t = 0.735$ s, $t = 0.854$ s, $t = 0.98$ s (second row).

6 Conclusions

An efficient computational model for the simulation of two-phases flows has been presented. It allows to consider both Newtonian and non-Newtonian flows. It relies on an Eulerian framework and couples finite element techniques with a forward characteristics method. Numerical results illustrate the large range of applications covered by the model. Extensions are being investigated (1) to couple viscoelastic and surface tension effects, (2) to reduce the CPU time required to solve Stokes problems, and (3) to improve the reconstruction of the interface and the computation of surface tension effects.

Acknowledgement. The authors wish to thank Vincent Maronnier for his contribution to this project and his implementation support.

References

[AMS04] E. Aulisa, S. Manservisi, and R. Scardovelli. A surface marker algorithm coupled to an area-preserving marker redistribution method for three-dimensional interface tracking. *J. Comput. Phys.*, 197(2):555–584, 2004.

[BCP06a] A. Bonito, Ph. Clément, and M. Picasso. Finite element analysis of a simplified stochastic Hookean dumbbells model arising from viscoelastic flows. *M2AN Math. Model. Numer. Anal.*, 40(4):785–814, 2006.

[BCP06b] A. Bonito, Ph. Clément, and M. Picasso. Mathematical analysis of a simplified Hookean dumbbells model arising from viscoelastic flows. *J. Evol. Equ.*, 6(3):381–398, 2006.

[BCP07] A. Bonito, Ph. Clément, and M. Picasso. Mathematical and numerical analysis of a simplified time-dependent viscoelastic flow. *Numer. Math.*, 107(2):213–255, 2007.

[BDJ80] R. B. Bird, N. L. Dotson, and N. L. Johnson. Polymer solution rheology based on a finitely extensible bead-spring chain model. *J. Non-Newtonian Fluid Mech.*, 7:213–235, 1980.

[BKZ92] J. U. Brackbill, D. B. Kothe, and C. Zemach. A continuum method for modeling surface tension. *J. Comput. Phys.*, 100:335–354, 1992.

[BPL06] A. Bonito, M. Picasso, and M. Laso. Numerical simulation of 3D viscoelastic flows with free surfaces. *J. Comput. Phys.*, 215(2):691–716, 2006.

[BPS01] J. Bonvin, M. Picasso, and R. Stenberg. GLS and EVSS methods for a three-field Stokes problem arising from viscoelastic flows. *Comput. Methods Appl. Mech. Engrg.*, 190(29–30):3893–3914, 2001.

[BRLH02] A. Bach, H. K. Rasmussen, P.-Y. Longin, and O. Hassager. Growth of non-axisymmetric disturbances of the free surface in the filament stretching rheometer: experiments and simulation. *J. Non-Newtonian Fluid Mech.*, 108:163–186, 2002.

[Cab05] A. Caboussat. Numerical simulation of two-phase free surface flows. *Arch. Comput. Methods Engrg.*, 12(2):165–210, 2005.

[Cab06] A. Caboussat. A numerical method for the simulation of free surface flows with surface tension. *Comput. & Fluids*, 35(10):1205–1216, 2006.

[CPR05] A. Caboussat, M. Picasso, and J. Rappaz. Numerical simulation of free surface incompressible liquid flows surrounded by compressible gas. *J. Comput. Phys.*, 203(2):626–649, 2005.

[CR05] A. Caboussat and J. Rappaz. Analysis of a one-dimensional free surface flow problem. *Numer. Math.*, 101(1):67–86, 2005.

[DLCB03] D. Derks, A. Lindner, C. Creton, and D. Bonn. Cohesive failure of thin layers of soft model adhesives under tension. *J. Appl. Phys.*, 93(3):1557–1566, 2003.

[FCD+06] M. M. Francois, S. J. Cummins, E. D. Dendy, D. B. Kothe, J. M. Sicilian, and M. W. Williams. A balanced-force algorithm for continuous and sharp interfacial surface tension models within a volume tracking framework. *J. Comput. Phys.*, 213(1):141–173, 2006.

[FF92] L. P. Franca and S. L. Frey. Stabilized finite element method: II. The incompressible Navier–Stokes equations. *Comput. Methods Appl. Mech. Engrg.*, 99:209–233, 1992.

[FGP97] M. Fortin, R. Guénette, and R. Pierre. Numerical analysis of the modified EVSS method. *Comput. Methods Appl. Mech. Engrg.*, 143(1–2):79–95, 1997.

[Gie82] H. Giesekus. A simple constitutive equation for polymer fluids based on the concept of deformation-dependent tensorial mobility. *J. Non-Newtonian Fluid Mech.*, 11(1–2):69–109, 1982.

[Glo03] R. Glowinski. Finite element methods for incompressible viscous flow. In P. G. Ciarlet and J.-L. Lions, editors, *Handbook of Numerical Analysis, Vol. IX*, pages 3–1176. North-Holland, Amsterdam, 2003.

[GLP03] E. Grande, M. Laso, and M. Picasso. Calculation of variable-topology free surface flows using CONNFFESSIT. *J. Non-Newtonian Fluid Mech.*, 113(2):123–145, 2003.

[Mar90] G. I. Marchuk. Splitting and alternating direction methods. In P. G. Ciarlet and J.-L. Lions, editors, *Handbook of Numerical Analysis, Vol. I*, pages 197–462. North-Holland, Amsterdam, 1990.

[Mau96] B. Maury. Characteristics ALE method for the 3D Navier-Stokes equations with a free surface. *Int. J. Comput. Fluid Dyn.*, 6:175–188, 1996.

[MPR99] V. Maronnier, M. Picasso, and J. Rappaz. Numerical simulation of free surface flows. *J. Comput. Phys.*, 155:439–455, 1999.

[MPR03] V. Maronnier, M. Picasso, and J. Rappaz. Numerical simulation of three dimensional free surface flows. *Internat. J. Numer. Methods Fluids*, 42(7):697–716, 2003.

[MS02] G. H. McKinley and T. Sridhar. Filament-stretching rheometry of complex fluids. *Ann. Rev. Fluid Mech.*, 34:375–415, 2002.

[NW76] W. F. Noh and P. Woodward. SLIC (Simple Line Interface Calculation). In A. I. van de Vooren and P. J. Zandbergen, editors, *Proc. of the 5th International Conference on Numerical Methods in Fluid Dynamics (Enschede, 1976)*, volume 59 of *Lectures Notes in Physics*, pages 330–340, Springer-Verlag, Berlin, 1976.

[OF01] S. Osher and R. P. Fedkiw. Level set methods: An overview and some recent results. *J. Comput. Phys.*, 169:463–502, 2001.

[Old50] J. G. Oldroyd. On the formulation of rheological equations of state. *Proc. Roy. Soc. London. Ser. A.*, 200(1063):523–541, 1950.

[Pir89] O. Pironneau. *Finite Element Methods for Fluids*. Wiley, Chichester, 1989.

[PR01] M. Picasso and J. Rappaz. Existence, a priori and a posteriori error estimates for a nonlinear three-field problem arising from Oldroyd-B viscoelastic flows. *M2AN Math. Model. Numer. Anal.*, 35(5):879–897, 2001.

[PTT77] N. Phan-Thien and R.I. Tanner. A new constitutive equation derived from network theory. *J. Non-Newtonian Fluid Mech.*, 2(4):353–365, 1977.

[RDG+00] M. Rappaz, J. L. Desbiolles, C. A. Gandin, S. Henry, A. Semoroz, and P. Thevoz. Modelling of solidification microstructures. *Mater. Sci. Forum*, 329(3):389–396, 2000.

[RH99] H. K. Rasmussen and O. Hassager. Three-dimensional simulations of viscoelastic instability in polymeric filaments. *J. Non-Newtonian Fluid Mech.*, 82:189–202, 1999.

[RK98] W. J. Rider and D. B. Kothe. Reconstructing volume tracking. *J. Comput. Phys.*, 141:112–152, 1998.

[Set96] J. A. Sethian. *Level Set Methods, Evolving Interfaces in Geometry, Fluid Mechanics, Computer Vision, and Material Science*. Monographs on Applied and Computational Mathematics. Cambridge University Press, 1996.

[SW04] M. Shashkov and B. Wendroff. The repair paradigm and application to conservation laws. *J. Comput. Phys.*, 198(1):265–277, 2004.

[SZ99] R. Scardovelli and S. Zaleski. Direct numerical simulation of free surface and interfacial flows. *Ann. Rev. Fluid Mech.*, 31:567–603, 1999.

[TMC+02] M. F. Tomé, N. Mangiavacchi, J. A. Cuminato, A. Castelo, and S. McKee. A finite difference technique for simulating unsteady viscoelastic free surface flows. *J. Non-Newtonian Fluid Mech.*, 106:61–106, 2002.

[War72] H. R. Warner. Kinetic theory and rheology of dilute suspensions of finitely extendible dumbbells. *Ind. Eng. Chem. Fund.*, 11:379–387, 1972.

[WKP99] M. W. Williams, D. B. Kothe, and E. G. Puckett. Accuracy and convergence of continuum surface tension models. In *Fluid Dynamics at Interfaces (Gainesville, FL, 1998)*, pages 294–305. Cambridge University Press, 1999.